NASA TECHNICAL NOTE

NASA TN D-4180

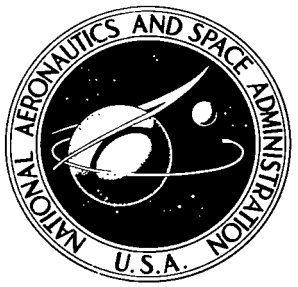

NASA TN D-4180

THEORETICAL AND PRACTICAL RESOLUTION LIMITS FOR PROCESSING PULSE FREQUENCY MODULATION TELEMETRY

by Thomas J. Karras and Paul Heffner

Goddard Space Flight Center
Greenbelt, Md.

NATIONAL AERONAUTICS AND SPACE ADMINISTRATION • WASHINGTON, D. C. • MARCH 1968

NASA TN D-4180

THEORETICAL AND PRACTICAL RESOLUTION LIMITS FOR PROCESSING PULSE FREQUENCY MODULATION TELEMETRY

By Thomas J. Karras and Paul Heffner

Goddard Space Flight Center
Greenbelt, Md.

NATIONAL AERONAUTICS AND SPACE ADMINISTRATION

For sale by the Clearinghouse for Federal Scientific and Technical Information
Springfield, Virginia 22151 – CFSTI price $3.00

ABSTRACT

The importance of knowing the meaning, methods of computation, and proper use of the equivalent noise bandwidth (ENBW) of a system is presented. From this, a normalized relation for expressing the signal energy per bit of information and the noise power density of the noise in the signal will be developed and compared to the most common S_{rms}/N_{rms} measurement.

A universal Pulse Frequency Modulation (PFM) telemetry data processing line (called F-8) has been operational at Goddard Space Flight Center (GSFC) since the launch of the Anchored Interplanetary Monitoring Platform-D (AIMP-D) satellite. The line incorporates two processing subsystems, a low resolution processor and a high resolution processor. The low resolution processor resolves the data measurement to 1 percent of the data spectrum, while the high resolution processor resolves the data measurement within 0.02 percent to 1 percent. The resolution given by the high resolution processor is a direct function of the input signal-to-noise ratio. The theoretical and actual performance of both modes of processing are described. Reference is made to three presently transmitting PFM satellites.

CONTENTS

THEORETICAL AND PRACTICAL RESOLUTION LIMITS FOR PROCESSING PULSE FREQUENCY MODULATION TELEMETRY

by
Thomas J. Karras and Paul Heffner
Goddard Space Flight Center

INTRODUCTION

When the ENBW of a system or a band limiting filter is not properly determined, there is often an error of as much as 2 db when experimental results are compared with theoretical calculations. Knowledge of ENBW or B and period per information bit (T/n) allows one to properly relate the concept of S/N versus probability of error with the concept of (ST/n)/(N/B) versus probability of error. This then establishes a mutual understanding of these concepts for any engineering community.

Actual test results obtained from the most recent production PFM line are compared with theoretical curves. Two detection systems within this PFM processor, one employing a high resolution processor (HRP) and one a more conventional comb filter system, are discussed. The HRP improves frequency resolution by an order of magnitude over the conventional comb filter system at high input signal-to-noise ratios. Adding a signal conditioner in the HRP system provides an additional 10-db improvement. The performance of the high resolution processor system is within 2 db of its theoretical curve as is the performance of the conventional comb filter system. These results are applicable to Energetic Particles Explorer-D (EPE-D), Anchored Interplanetary Monitoring Platform-D (AIMP-D), and Advanced Technological Satellite-B (ATS-B), which are presently transmitting PFM telemetry.

PULSE FREQUENCY MODULATION TELEMETRY

PFM telemetry is widely used on GSFC scientific satellites. Conventional PFM is a system whereby the information of each channel in a telemeter determines the frequency of a subcarrier oscillator whose burst duration is nominally 10 milliseconds (ms). Each 10-ms burst is preceded by a 10-ms blank for burst-blank format, a 10-ms reference frequency for burst-reference PFM, or another 10-ms data burst for burst-burst PFM. Figure 1 indicates three standard PFM formats used for AIMP-D, ATS-B, and EPE-D satellites presently orbiting the earth.

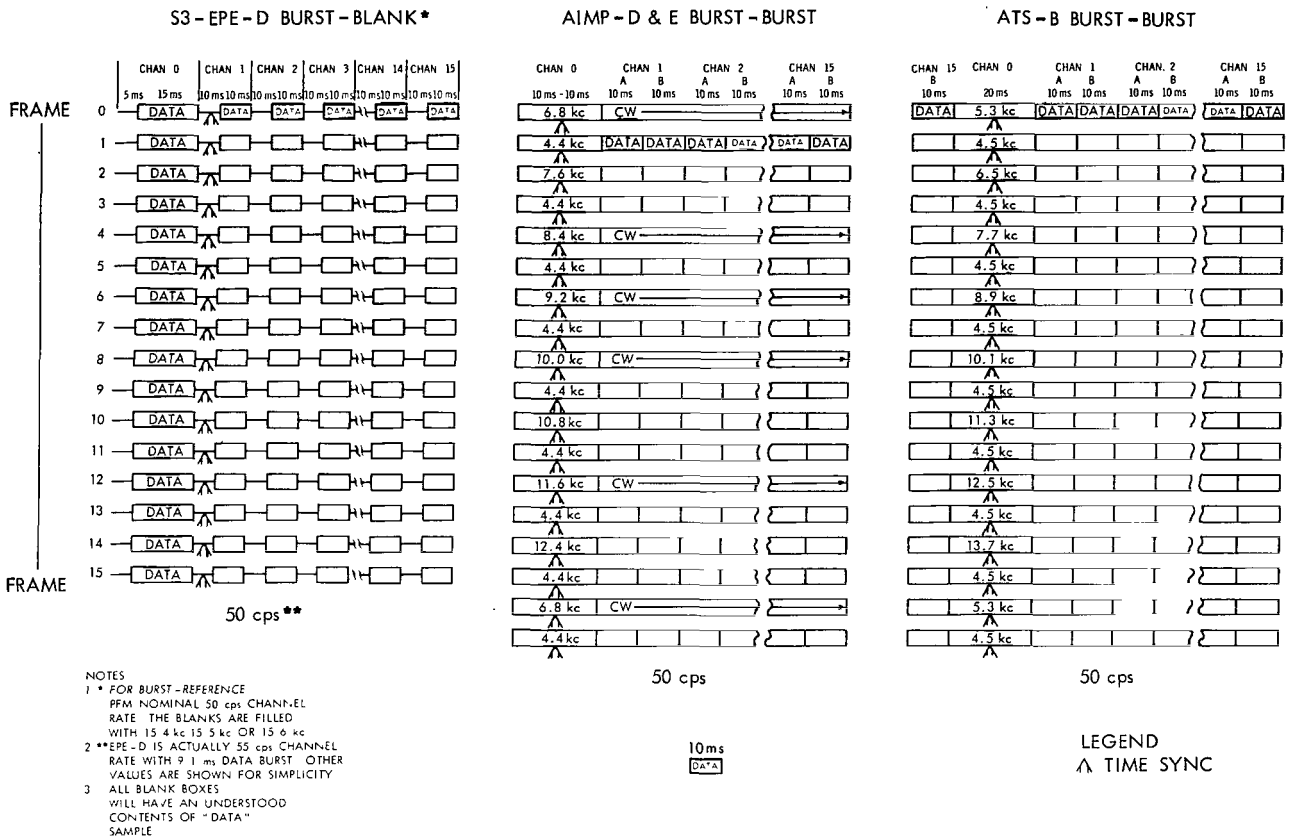

Figure 1—Standard PFM formats used for AIMP-D, ATS-B, and EPE-D satellites.

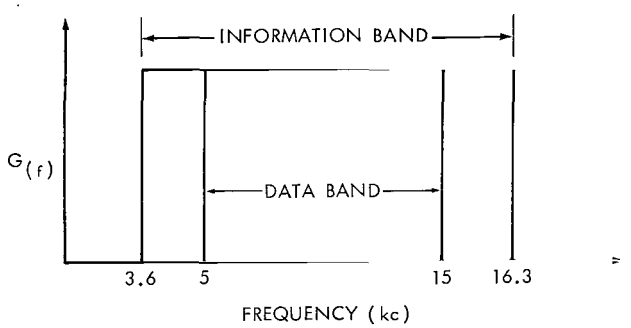

Figure 2—Nominal PFM data spectrum.

There are 16 channel pairs* of information in each frame of data. The first channel pair at the beginning of each frame (20 ms) usually contains a known frequency used for frame or channel synchronization. There are 16 frames per sequence. The nominal data frequency can be anywhere in the frequency range of 5 to 15 kc (see Figure 2). The total information band is 3.6 to 16.3 kc (12.7 kc).

INTERPRETATION OF EQUIVALENT NOISE BANDWIDTH

The terms "bandwidth" and "noise bandwidth" are not in themselves complete or correct to use in the engineering field. A better expression might be "3-db bandwidth" or "3-db noise bandwidth." However, this expression is still not sufficient since one would also need such information as the filter roll off characteristics, passband ripple, and phase shift characteristics.

*A channel pair is used here to represent the blank-burst, reference-burst, or burst-burst channel.

The term ENBW is perhaps most useful when one is performing a theoretical study on laboratory testing of system performance. The term is also useful to express the noise power (from a white noise source) which would pass through a systems filter regardless of the shape of that filter's response curve. The ENBW is the bandwidth of an ideal rectangular filter which would pass the same amount of white noise power as the filter to which the ENBW refers. Knowledge of the ENBW of a filter facilitates (1) computation of the signal-to-noise ratio improvement offered by the filter when used in a system, (2) direct comparison of one system's test results with those of another, (3) or comparison with the same system tested in a different laboratory environment, such as use of different noise generators or testing devices.

The basic relationships which can be used for computing the ENBW for positive frequencies (one-sided ENBW) given the filter or system transfer function $H(j\omega)$ are as follows:

Low-pass Filter:

$$\text{ENBW(rad/sec)} = \frac{\int_0^\infty |H(j\omega)|^2 \, d\omega}{|H(j\omega)|^2_{\omega \to 0}}, \tag{1}$$

where ω is in rad/sec.

Band-pass Filter:

$$\text{ENBW(rad/sec)} = \frac{\int_0^\infty |H(j\omega)|^2 \, d\omega}{|H(j\omega)|^2_{max}}. \tag{2}$$

High-pass Filter:

$$\text{ENBW(rad/sec)} = \frac{\int_0^\infty |H(j\omega)|^2 \, d\omega}{|H(j\omega)|^2_{\omega \to \infty}}. \tag{3}$$

More detailed information on the computations for ENBW are found in Reference 1.

The use of the ENBW can be demonstrated by considering the processing of PFM data by comb filters. Let a filter within the comb be a single-pole, band-pass filter with a 3-db bandwidth of 100 cps, and let each filter be separated by 100 cycles in center frequency from an adjacent filter. Figure 3 shows one such filter within the comb filter, used when the data frequencies range between 5 and 15 kc. In theory, one refers to a rectangular filter which has the same maximum gain and which passes the same average noise power from a white noise source as the "single-pole filter." The bandwidth of this ideal rectangular filter is called its equivalent noise bandwidth. Since the

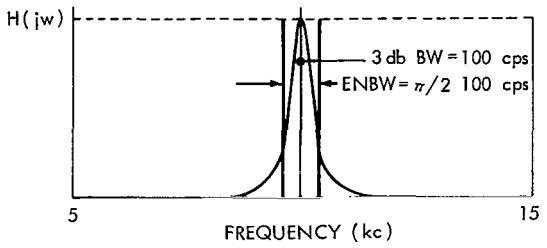

Figure 3—Single-pole filter with its equivalent rectangular filter.

data frequency can be between 5 and 15 kc, the bandwidth of the noise passing into the comb filter is at least 10 kc. (See Appendix A for a description of a comb filter.)

The signal-to-noise improvement of the single-pole filter in this comb filter is found by computing (S/N) improvement = $(S/N)_{out}/(S/N)_{in}$. Assuming that the input frequency is at the center of the filter ($S_{in} = S_0$), then, the improvement becomes:

$$\frac{(S/N)_{out}}{(S/N)_{in}} = 10 \log \left(\frac{\text{noise power input to the comb filter}}{\text{noise power passing through a single pole filter}} \right) \quad (4)$$

$$= 10 \log \frac{10,000}{\text{ENBW}^*} \quad (5)$$

$$= 10 \log \frac{10,000 \text{ cps}}{\frac{\pi}{2} 100 \text{ cps}} \approx 18\text{-db improvement} .$$

If the input frequency is offset from the filter center frequency, the signal-to-noise ratio improvement becomes less than +18 db, since $S_0 < S_{in}$ along the skirts of the filter. For example, the improvement would be +15 db if the input frequency is at the crossover (3 db) point.

If one uses the 100 cps f_{3db} bandwidth for the ENBW of a single-pole filter in Equation 5, the resultant error would be 10 log $2/\pi$ or 2 db. A single RC low-pass filter with a 3-db bandwidth of f_{3db} also has an ENBW of $\pi/2$ f_{3db}. Hence, if one simply places an RC low-pass filter at the output of a wideband noise generator, he immediately knows the ENBW of the noise presented to a system under test and can relate his results to theoretical or other test results.

Present day noise generators used in the laboratory having a switch setting labeled 20 kc actually have an ENBW of approximately 70 kc. Hence, an error of 10 log (70 kc/20 kc) or 5.5 db would exist if one implied on his experimental data that his ENBW was 20 kc (this assumes that no external filter is employed to band limit the noise).

S/N VS (ST/n)/(N/B)

A normalized relation can be established for a PFM signal mixed with band limited Gaussian noise. This relation serves as a basis by which the probability of success (or error) can be plotted

*By use of Equation 2, the ENBW for a single-pole RLC tuned-bandpass filter is shown in Reference 1 to be $\pi/2$ f_{3db}.

for a particular system or transmission technique. By plotting curves for other systems or transmission techniques, a direct comparison of performance can be made.

The relation of interest, given in decibels, is defined as follows:

$$\left[\frac{\text{Signal energy per bit}}{\text{Noise power density}}\right]_{db} = \left[\frac{S_p\, T/n}{N_p/B}\right]_{db} = 10 \log_{10} \frac{S_p\, T/n}{N_p/B}, \tag{6}$$

where

S_p = signal power in watts

N_p = noise power in watts

B = ENBW in cps

T/n = equivalent period between bits in (sec/bit).

Inspection of a separation of this relation allows easy interpretation of trends that are affected by varying different parameters

$$\frac{\text{Signal energy per bit}}{\text{Noise power density}} \quad 10 \log \left(\frac{S_p}{N_p}\right) + 10 \log \frac{BT}{n}, \tag{7}$$

where (S_p/N_p) is the usual variable with time and (BT/n) is usually defined by the technique or system employed.

Figure 4 illustrates the dependence of $(ST/n)/(N/B)$ on S/N for n = 7 (a 128-level system) and for various values of B for T = 0.01 for the 10-ms burst PFM signal. The term TB/n is the term used when translating a $(ST/n)/(N/B)$ curve to a S/N curve or vice versa. For the theoretical and actual resultant curves of system performances given in this paper, this translation is 14.6 db, as can be seen on the curve representing an ENBW = 20 kc.

As a translation example, consider a hypothetical case where a resultant test curve was generated from tests made on a system (see Figure 5 (a)). The signal was PFM, having a burst width of 10 ms; the noise was Gaussian, having an ENBW = 40 kc. The system was a 128-level system (n = 7).

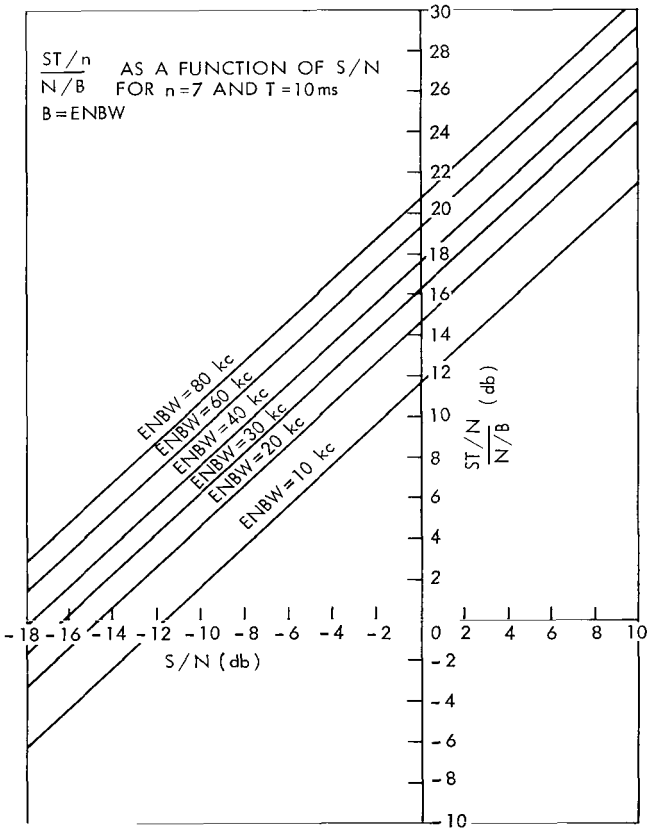

Figure 4—Energy per bit per noise power density versus RMS signal-to-noise ratios.

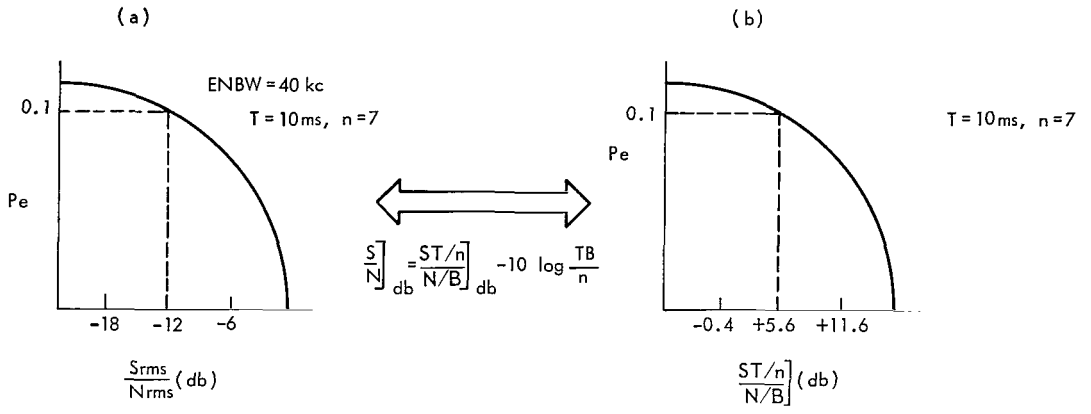

Figure 5—Example of translation between S/N and (ST/n)/(N/B) curves.

Using Figure 4 and the 40-kc ENBW case, a translation is made from a -12 db of signal-to-noise to +5.6 db of (ST/n)/(N/B); likewise -6 db is translated to +11.6 db and -18 db to -0.4 db. From this, Figure (b) is generated. The translation could have been calculated by

$$10 \log_{10} \frac{BT}{n} = 10 \log \frac{40 \times 10^3 \times 10^{-2}}{7} = 17.6 \text{ db} ,$$

and using the following expression:

$$\frac{S_{rms}}{N_{rms}} = \frac{ST/n}{N/B} - 10 \log_{10} \frac{TB}{n} . \tag{8}$$

THEORETICAL AND ACTUAL LOW RESOLUTION PROCESSING PERFORMANCE

Low resolution processing (LRP) of PFM telemetry is presently performed at the GSFC with a bank of 128 contiguous filter elements (comb filter). Each filter element is followed by a threshold detector. The nominal frequency range covered by the comb filter is 3.6 to 16.3 kc which is the range required for frame and channel synchronization information along with guard band frequencies. The frequency of the experimenter's data normally can be anywhere in the range of 5 to 15 kc.

Each of the filters ia a single-pole, narrow bandpass crystal filter element with a 3-db bandwidth of 100 cps and a center frequency separation of 100 cps. Thus, the incoming 10-kc data band is only resolved to 1 of 100 possibilities or provides a resolution of 1 percent regardless of the input signal-to-noise ratio. The incoming signal causes the appropriate filter to respond beyond a given threshold, causing all other filters to be inhibited.

The maximum output signal-to-noise improvement mentioned earlier, assuming 10-kc input ENBW, is 18 db. Assuming that the input frequency can lie anywhere within the 100-cps bandwidth

with equal probability, then the average signal-to-noise improvement is 17 db. If the input ENBW is 20 kc in the telemetry link, the average signal-to-noise improvement will be 20 db.

Figure 6 is the actual LRP performance curve obtained from simulated burst–burst PFM random data added with White Gaussian noise bandlimited with a 20-kc ENBW filter for various signal-to-noise ratios. The processing line used the 4.4-kc channel O frame synchronization tone shown on Figure 1 to obtain channel synchronization.

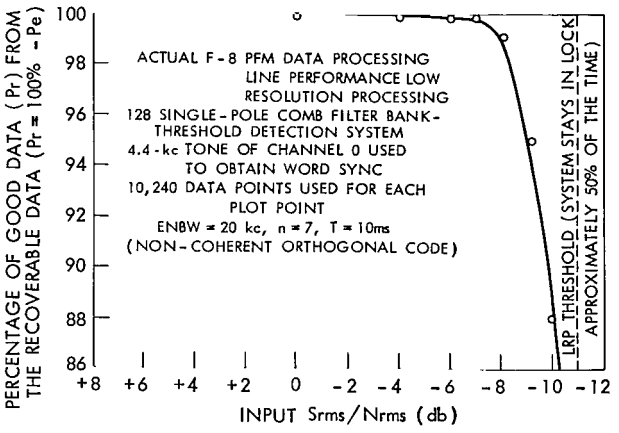

Figure 6—Actual F-8 PFM data processing line performance.

Figure 7-D plotted as the probability of word error versus (ST/n)/(N/B), is a translation of the F-8 actual performance as given in Figure 6. Each value* on Figure 6 added to 10 log TB/n (14.6 db) translates the F-8 actual performance curve to Figure 7-D. Compared to the actual performance curve obtained for random simulated data are three theoretical curves labeled A, B, and C in Figure 7. Theoretical curves A and B were obtained from Reference 2.

Theoretical curve A, Figure 7 is plotted from the following expression of word error probability for orthogonal codes:

$$P_e = 1 - \int_{-\infty}^{\infty} \left(\frac{1}{\sqrt{2\pi}\,\sigma} \int_{-\infty}^{x_0} e^{-x^2/2\sigma^2}\, dx \right)^{127} \left(\frac{1}{\sqrt{2\pi}\,\sigma} e^{-(x_0 - C_0)^2/2\sigma^2}\, dx_0 \right) , \qquad (9)$$

where C_0 and σ are the signal and noise rms value over the distribution of x. The model used was a matched filter followed by a maximum likelihood detection system.

Theoretical curve B is plotted from the following expression of word error probability for orthogonal codes:

$$P_e = 1 - \int_0^{\infty} \left\{ \frac{1}{\sigma^2} \int_0^{r_0} r e^{-r^2/2\sigma^2}\, dr \right\}^{127} \cdot \frac{r_0}{\sigma^2} e^{-r_0^2 + C_0^2/2\sigma^2} \frac{1}{2\pi} \int_0^{2\pi} e^{r_0 C_0 \cos(\theta - \theta_0)/\sigma^2}\, d\theta\, dr_0 \qquad (10)$$

where r and θ are polar coordinates as opposed to rectangular x of Equation 9. The model used was an ideal rectangular filter (100-cps bandwidth) followed by a maximum likelihood detection system.

*Figure 6 is plotted as P(success) = $P_r = 1 - P_e$; Figure 7 is plotted as P_e.

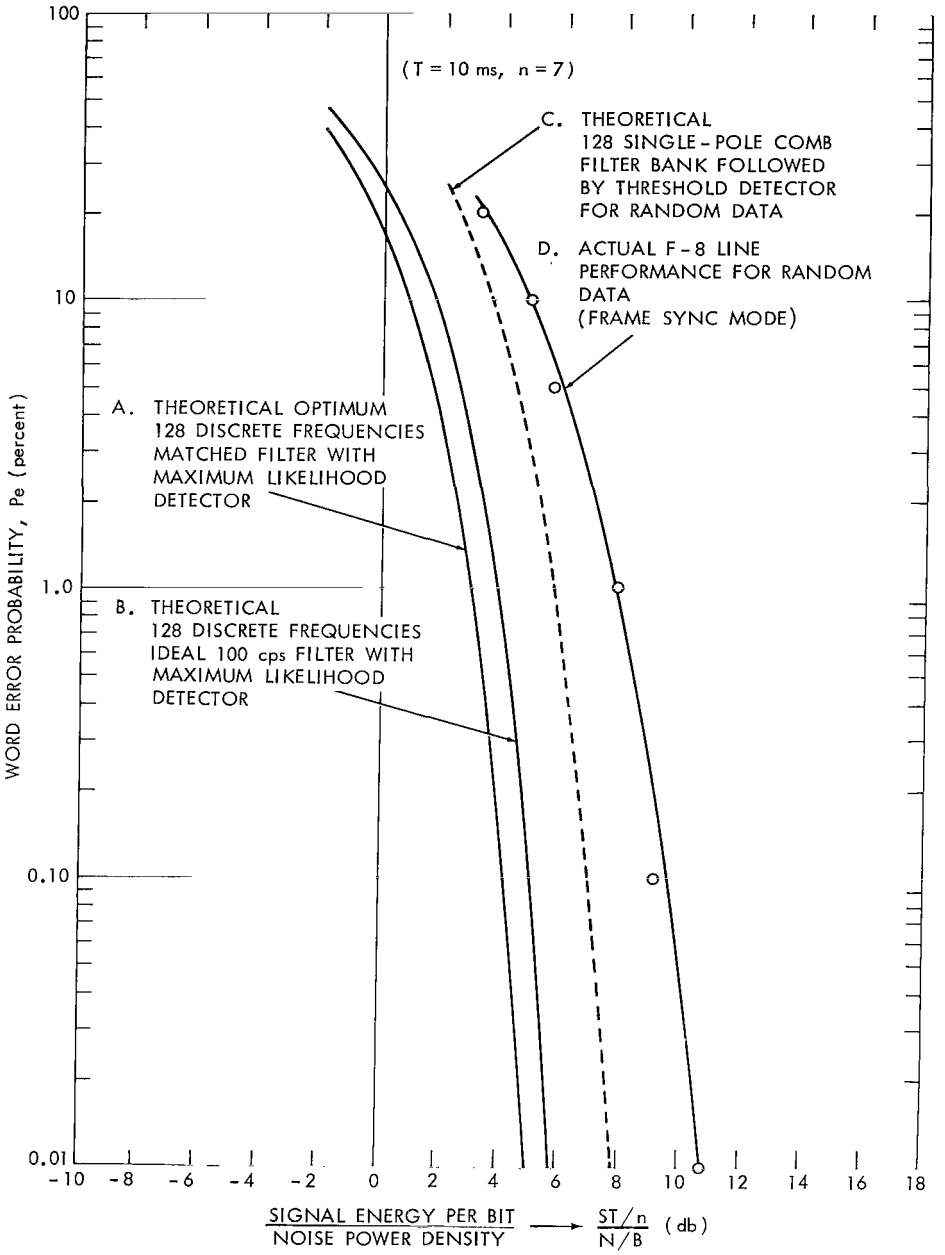

Figure 7—Word error probability for orthogonal codes.

Theoretical curve C for the comb filter used in the processing lines differs by 2 db from theoretical curve B because: (1) the comb filter does not employ ideal filters followed by maximum likelihood detectors, and (2) the comb filter, on the average, provides 1-db less improvement than would be provided if all frequencies fell in the centers of each bandpass filter.

The actual performance curve D for the F-8 line is within 2 db of the theoretical curve C for the comb filter bank-threshold detection system. It is believed that this difference results principally

from the lack of perfect synchronization employed by using the frame sync burst every other frame for obtaining channel synchronization.

From the viewpoint of high resolution processing a major disadvantage of employing a fixed bank of 100 filters to cover the 10-kc data band is that one can only know the incoming frequencies to 1 percent, regardless of the input signal-to-noise ratio. With this filter bank principle, smaller quantizations can be obtained by using more filters with narrower bandwidths. This practice becomes not only excessively expensive, but also operationally cumbersome. For example, a 0.1 percent resolution would require 1000 filters each with a bandwidth of 10 cps. This would introduce the complication that the buildup time for a 10-cps filter would be approximately 100 ms. Therefore, the buildup would not be compatible with standard PFM, unless the filters were quenched or dumped. Especially critical for high resolution is the fact that the filter bank is not tape speed compensated. Hence, the development of a HRP operating on a different principle from the LRP was adopted.

THEORETICAL AND ACTUAL HIGH RESOLUTION PROCESSING PERFORMANCE

When more accurate measurements (better than 1 percent) of the incoming frequencies are necessary, a means other than a large bank of contiguous filters is employed to take advantage of the quality of the available signal. For this reason high resolution processing is presently being used, in addition to low resolution processing, for simultaneous reduction of PFM telemetry at GSFC.

The frequency measurement technique employed (Reference 3) is a method whereby an elapsed time of data cycles is measured by a high frequency reference count z, where y is the integral number of data cycles plus one that elapsed in a preset time interval. The high frequency reference count is tape speed compensated. A characteristic of this method is that the resolution of the measurement is dependent upon the incoming signal-to-noise ratio and is independent of the data frequency.* (Appendix B contains a brief description of the HRP.) The frequency measurement is then provided by a division routine performed by a logical divider within the system

$$f = \frac{5y}{z} \times 10^6 \text{ cps} , \tag{11}$$

where

y = number of data cycles +1 that occur in a preset time interval

z = number of 5 mc tape speed compensated reference frequency counts that occurred in the period of y data cycle counts.

*Resolution as used in the discussed systems is the difference between the measured frequency and the true frequency as related to the 10-kc data band.

Since noise is the limiting factor on the resolution of measurement, it is advantageous to reject as much of the noise mixed with the signal as possible before the actual measurement.

The method chosen to condition the PFM signal before frequency measurement was that of using a contiguous bank of gated filters (called Signal D comb filter).* The optimum choice for a filter bank (Reference 4) in the 10-kc data band resulted in 25 double-pole, Gaussian shaped filters with a 3-db bandwidth of 500 cps. These filters are arranged in a contiguous manner so that their attenuation characteristics overlap at the 1.5-db points. They are separated in center frequency of 400 cps. Incorporation of the sync and guard band frequencies resulted in a total of 32 filters or one-fourth as many filters as employed in the LRP system. The Signal D comb filter improves the signal-to-noise ratio by approximately 10 db (ENBW = 10 kc of the input noise) before the signal measurement. This filter bank not only allows for higher resolution of measurement at a given signal-to-noise ratio, but also lowers the threshold of the measuring device from +9 db to nearly -1 db signal-to-noise ratio (see Figure 8). Appendix C contains a brief description of the Signal D comb filter.

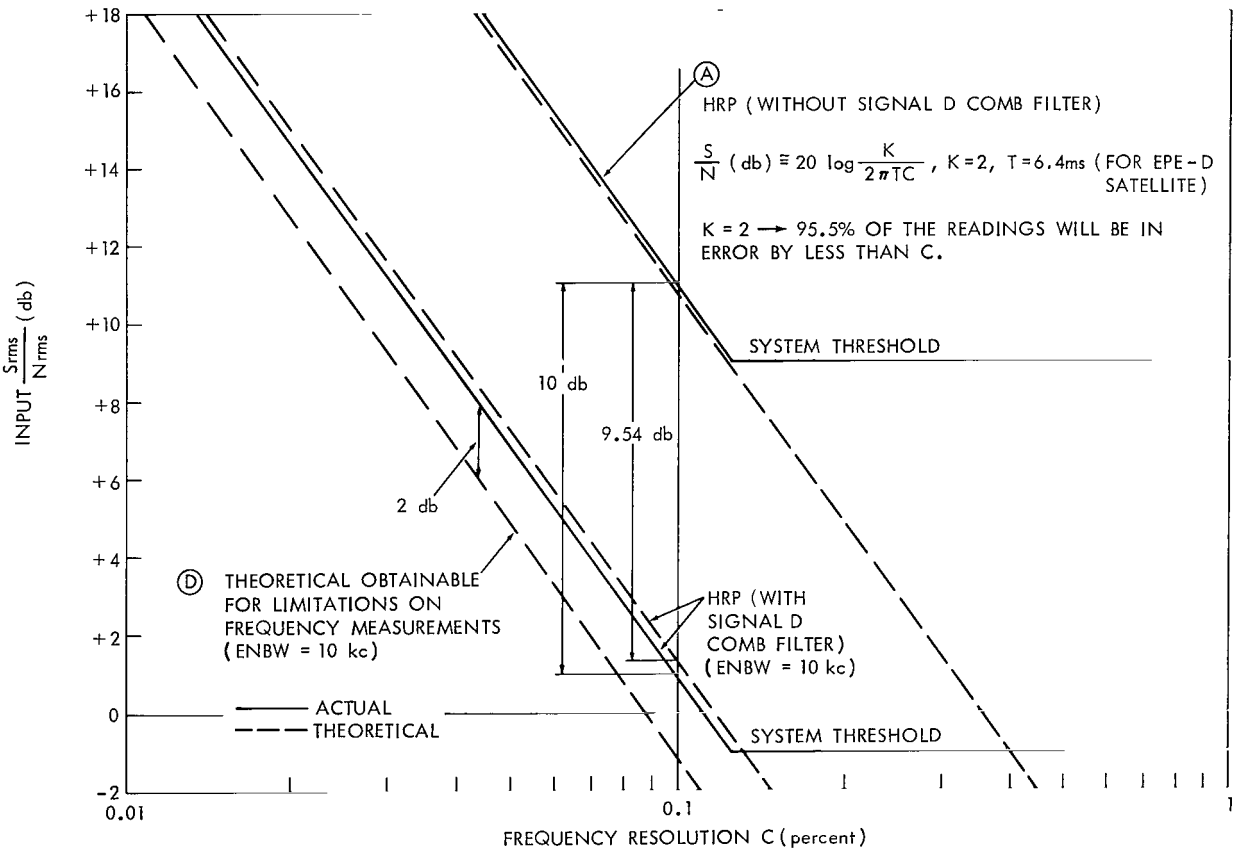

Figure 8—HRP performance curves.

*Karras, T. J., "Operation and Maintenance Manual for the Signal D Comb Filter," GSFC Document X-563-65-418, October 1965.

The relationship governing the HRP which makes frequency measurements over a nearly constant time interval regardless of frequency is as follows:

$$S/N(db) \cong 20 \log \left(\frac{K}{2\pi TC}\right), \tag{12}$$

where

K = confidence factor

T = measurement time

C = frequency resolution.

The expression is plotted as curve A in Figure 8.

The Signal D comb filter theoretically improves the signal-to-noise ratio by 9.54 db (10 db in actual measurements). The expression for the HRP then becomes:

$$S/N \cong 20 \log \frac{K}{2\pi TC} - 9.54 \text{ db} . \tag{13}$$

Metzner (Reference 5) set out to investigate other means of frequency measurements. A mathematical model was assumed using Signal Space concepts. The relationship developed yields the following rms frequency measurements error:

$$\sigma = \frac{1}{2\sqrt{3}} \left(1 + \frac{S}{N}\right)^{-TB} . \tag{14}$$

This expression is plotted in Figure 8. As indicated, the Signal D comb filter signal conditioner agrees within 2 db of the theoretical optimum obtainable from the Signal Space Model.

Other methods considered and summarized in Reference 6 have inherent serious limitations. The models chosen were: (1) statistical inputs of the frequency measurement problem, such as those connected with zero-crossings and maximum likelihood estimations; (2) the use of the phase-locked loop in frequency measurement; and (3) the effect of heterodyning on zero-crossing estimation.

Figure 9 is a plot of HRP performance for this subsystem, giving the threshold and the resolution of frequency measurement as functions of signal-to-noise ratio. The left ordinate is scaled to give resolution as a function of signal-to-noise ratio for a PFM signal in Gaussian noise having an ENBW of 20 kc. The k = 1 curve is the curve representing the rms value of the resolution within which 68 percent of all measurements will be limited. For the k = 2 curve, 95 percent of all measurements are confined to the given resolution. The quantization error, a direct function of a 5-Mc reference frequency and the 1 ms* sampling time will provide, in worst case, a 0.02 percent error in the frequency measurement. The rms value of this quantization error (which has a rectangular distribution) is 0.0082 percent. This then reflects a frequency dependent error as shown at the top left corner of Figure 9. The magnitude of this error for a particular frequency should be added to the resolution curve for actual performance.

*4 ms equivalent to real time.

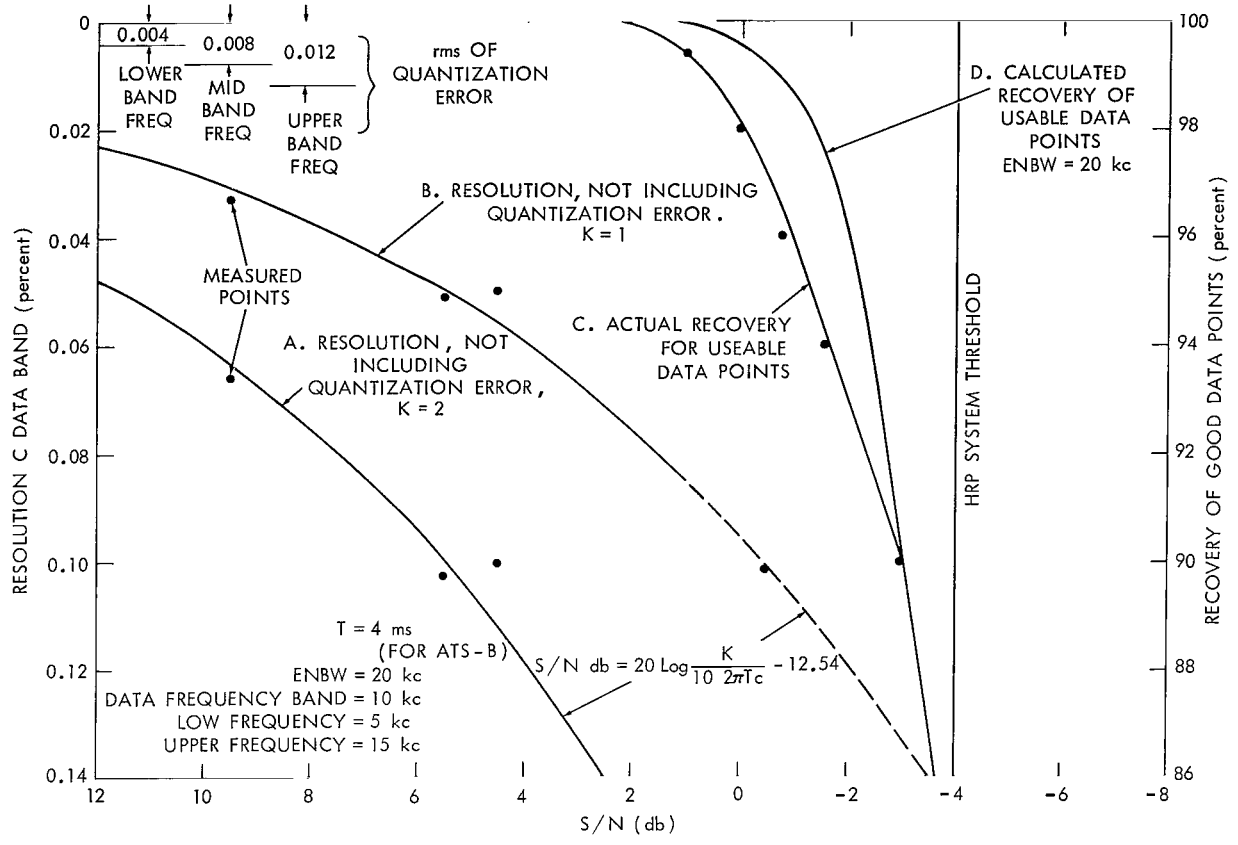

Figure 9—HRP theoretical and actual performance.

Curves C and D and the right ordinate of Figure 9 give the expected recovery of usable data points for this subsystem. This figure represents the threshold of the system because an unusable data point will exhibit a radical departure from the true frequency. This is due to failure of the zero crossing and counting technique to count every zero crossing or to count too many excursions. Curve D, Figure 9, is partially empirical and partially theoretical. It is based on a PFM signal in Gaussian noise with an ENBW of 20 kc. Curve C, the actual recovery curve, disagrees with the calculated curve by approximately 1-1/2 db in the region of interest.

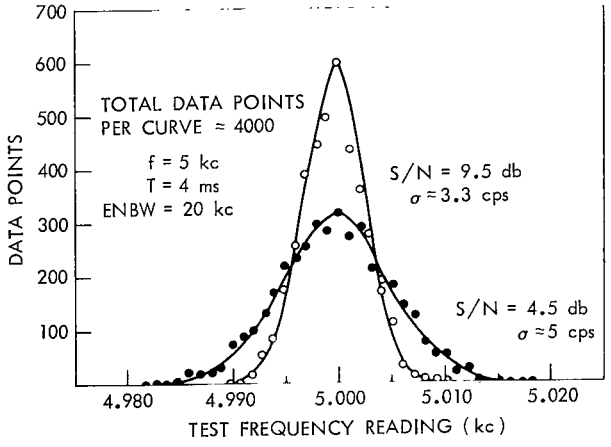

Figure 10—Probability density distribution of two sets of frequency measurement.

Curves A and B of Figure 9 are the most informative theoretical curves for predicting performance of the HRP for various signal-to-noise ratios. Test results shown on this figure were based on results such as those shown in Figure 10.

Figure 11 shows the consolidation of the actual recovery curves for both the HRP and the LRP. These two curves will determine the usefulness of either the HRP or LRP for predicted signal-to-noise ratios. The graph includes the expected worst case signal-to-noise ratios for three currently transmitting satellites (AIMP-D, ATS-B, and EPE-D). Prediction of these ratios necessitates a tabulation of the spacecraft transmitting power and the accumulative gains and losses for the signal before final processing. Also required is the expected noise power within a specified equivalent noise bandwidth. Appendix D gives a sample calculation of the predicted signal-to-noise ratio of AIMP-D at apogee.

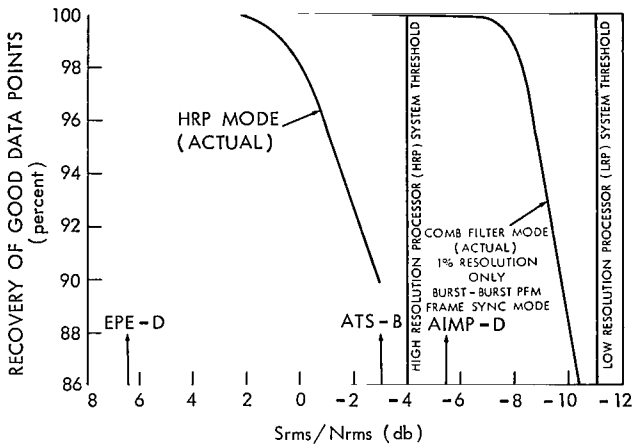

Figure 11—F-8 PFM line performance for HRP and LRP percent good data vs S/N (ENBW = 20 kc).

SYNCHRONIZER PERFORMANCE FOR PFM TELEMETRY

The PFM channel synchronizer in the F-8 Data Processing Line was tested separately for burst-blank, burst-reference, and burst-burst PFM telemetry synchronization signals available either in the format or in the LRP comb filter. Four test windows were placed around the synchronizer channel clock and the synchronizer filter performance was measured.*

Table 1 summarizes the performance of the PFM synchronizer at a 99.8-percent data recovery threshold occurring at -6 db for frame sync mode 4 for the four synchronizing methods.

*Karras, T. J., and Barnes, W. P., "Performance Test on Various Synchronizing Methods for Burst-Blank, Burst-Reference, and Burst-Burst PFM Telemetry," DIDB Technical Memorandum No. 1, Information Processing Division, GSFC, NASA.

Table 1
PFM Synchronizer Performance*

Mode — Synchronizer Method	Relative Synchronizer Threshold at 10% RMS jitter† Using Burst-Blank PFM as a Reference
1. Burst-reference PFM (using reference frequency for synchronization)	+1 db
2. Burst-blank PFM (using 50-cps signal from LRP comb filter AGC bus for synchronization)	0
3. Burst-burst PFM (using 100-cps signal from LRP comb filter AGC bus for synchronization, best data content used)	-3 db
4. Burst-burst PFM (using frame sync for synchronization)	-7 db

*At a 99.8% data recovery threshold occurring at -6 db for frame sync mode 4.
†At 10% 2σ rms jitter (95.5% of the time the synchronizer jitter is within ±2 ms), once the system finds lock for frame sync mode 4, it will continue to remain in lock.

At signal-to-noise ratios where the synchronizer jitter distribution was such that 2σ was equal to 10 percent of the channel period (20 percent of a 10-ms data burst) the following table was constructed. Burst-blank PFM is used as a reference. A positive db implies better performance.

Figure 12 shows the PFM line performance for sync and data recovery with various sync strategies and PFM data formats. It can be seen that the frame sync threshold, for which 50 percent

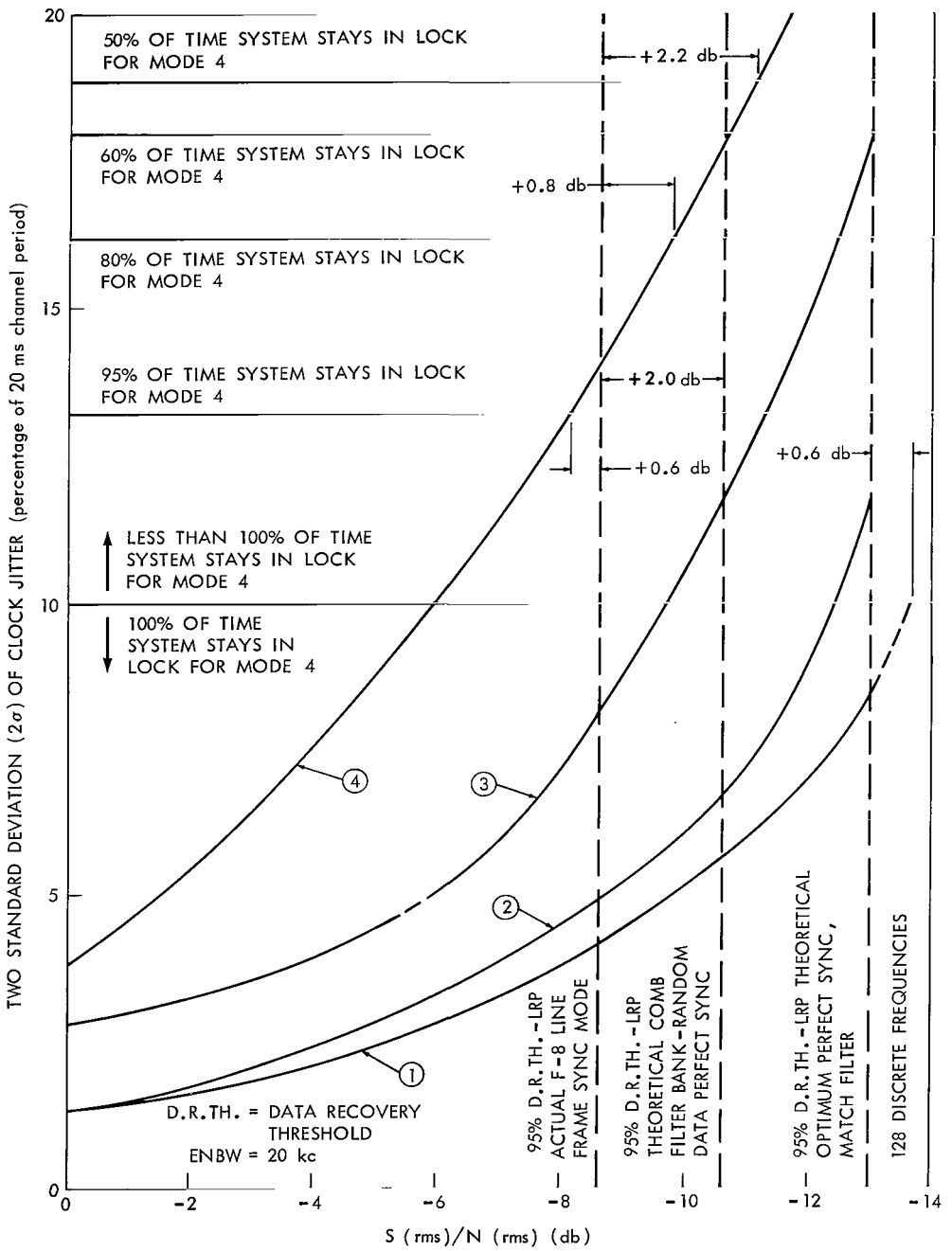

Figure 12—PFM synchronizer performance for four modes of synchronization.

of the time the system stays in lock, is approximately 2.2 db below the 95-percent data recovery threshold of the line. If a more nearly optimum and reliable sync mode for burst-burst data were used, up to a 2-db improvement (Data Recovery) could be obtained.

As shown in Figure 12, burst-reference PFM (with reference frequency used for sync) would be the optimum sync method for obtaining maximum data recovery. If, for example, 95 percent data recovery is desirable at -13 db (theoretical optimum obtained using matched filters and maximum likelihood detection), then burst-reference PFM and sync mode 1 must be employed in order that the sync threshold be lower than the data recovery threshold. However, even with the best sync information available, with matched filters, the sync threshold is only +0.6 db below the 95 percent data recovery threshold.

Synchronizer method four in Table 1 is employed in the F-8 PFM processor for burst-burst data because the synchronizer performance in this mode is independent of telemetry data content. If the telemetry data content were guaranteed to be different in frequency from burst-to-burst (eliminating inter-burst distortion), then method three would be 4 db superior to method four and certainly would be the method to use.

CONCLUSIONS

The two techniques employed by the present PFM processing line being used at GSFC were given. Basically, these techniques serve (1) to provide 1-percent resolution for a large range of input signal-to-noise ratios, and (2) to provide between 0.02-percent and 1-percent resolution depending upon the signal-to-noise ratio of the input signal when the ratio is high enough to utilize the HRP technique. It was shown that the thresholds of the two systems using the given techniques differ by approximately 8 db in effective input signal-to-noise ratios.

The signal-to-noise and (ST/n)/(N/B) theoretical curves for these systems were given and experimental results compared with the curves, using given measurement criteria. This criteria included the application of equivalent noise bandwidth for filter bandlimited white gaussian noise and the period per information bit being tested. Proper knowledge of ENBW (B) of a system under test and the period per information bit (T/n) of a signal allows one to translate between the signal-to-noise ratios and (ST/n)/(N/B) versus probability error curves.

The presently used 1-percent system employing a comb filter threshold detection technique was shown to be 5 db removed from the optimum system employing a matched filter and maximum likelihood detection system. The 1-percent system was shown to agree within 2 db of its theoretical curve. Likewise, measurements made on the high resolution system agreed within 2 db of its theoretical curve.

The channel synchronizing performance was given, and from these results the following conclusions were drawn. Burst-reference PFM provides the best synchronization performance over burst-blank and burst-burst PFM. However, it was concluded that even if an optimum detection

system were employed for burst-reference, a degradation in the probability of success would result since the synchronization threshold is only 1 db lower than the data recovery threshold in the region of interest.

Goddard Space Flight Center
National Aeronautics and Space Administration
Greenbelt, Maryland, June 30, 1967
125-23-02-00-51

REFERENCES

1. Karras, T. J., "Equivalent Noise Bandwidth Analysis from Transfer Functions," NASA Technical Note D-2842, November 1965.

2. Rochelle, R. W., "Pulse Frequency Modulation Telemetry," NASA Technical Report R-189, January 1964.

3. Demmerle, A. M., and Heffner, P., "The Resolution of Frequency Measurements in PFM Telemetry," NASA Technical Note D-2217, December 1964.

4. Demmerle, A. M., and Karras, T. J., "Signal Conditioning to Improve High Resolution Processing for PFM Telemetry," NASA Technical Note D-3057, May 1966.

5. Metzner, J. J., "Theoretical Limitations on the Accuracy of Frequency Measurements," New York University Technical Memorandum No. 56, February 1966.

6. Schwartz, L. S., "Frequency Measurement in the Presence of Noise," New York University Technical Memorandum No. 57, February 1966.

Appendix A

The Low Resolution Processor Comb Filter-Threshold Detection System

Figure A1 is a block diagram of the contiguous comb filter bank. The 3.6- to 16.3-kc incoming PFM signal is translated to 253.6 to 266.3 kc by an internal local oscillator of 250 kc. This facilitates using crystal filters having a 100-cps, 3-db bandwidth. Each filter is followed by a Schmitt Trigger which has a threshold setting equal to 60 percent of the maximum value of the filter-detected envelope. When one Schmitt Trigger has turned on, the thresholds of the other 127 Schmitt Triggers are raised. When the original envelope (which caused the Schmitt Trigger to be turned on) drops to 40 percent of its maximum value, all thresholds will again be at their 60-percent value. The output of the comb filters consists of the individual 128 Schmitt Trigger Levels which are all strobed near the end of the data burst for frequency detection.

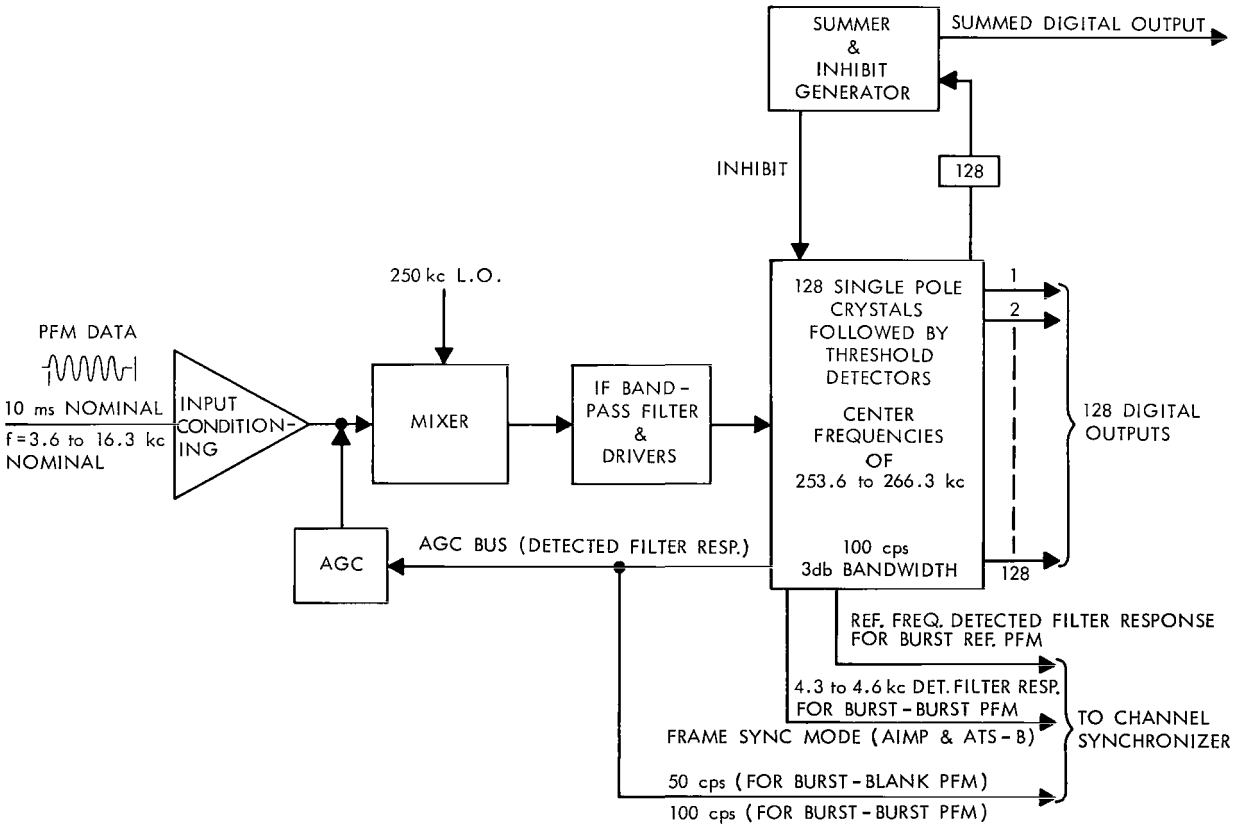

Figure A1—Low resolution processor comb filter block diagram.

Appendix B

HRP Frequency Measurement Subsystem

The HRP frequency measurement subsystem (Figure B1) measures the elapsed time of y cycles, where y is the integral number of cycles plus one that elapsed in a preset time interval. The

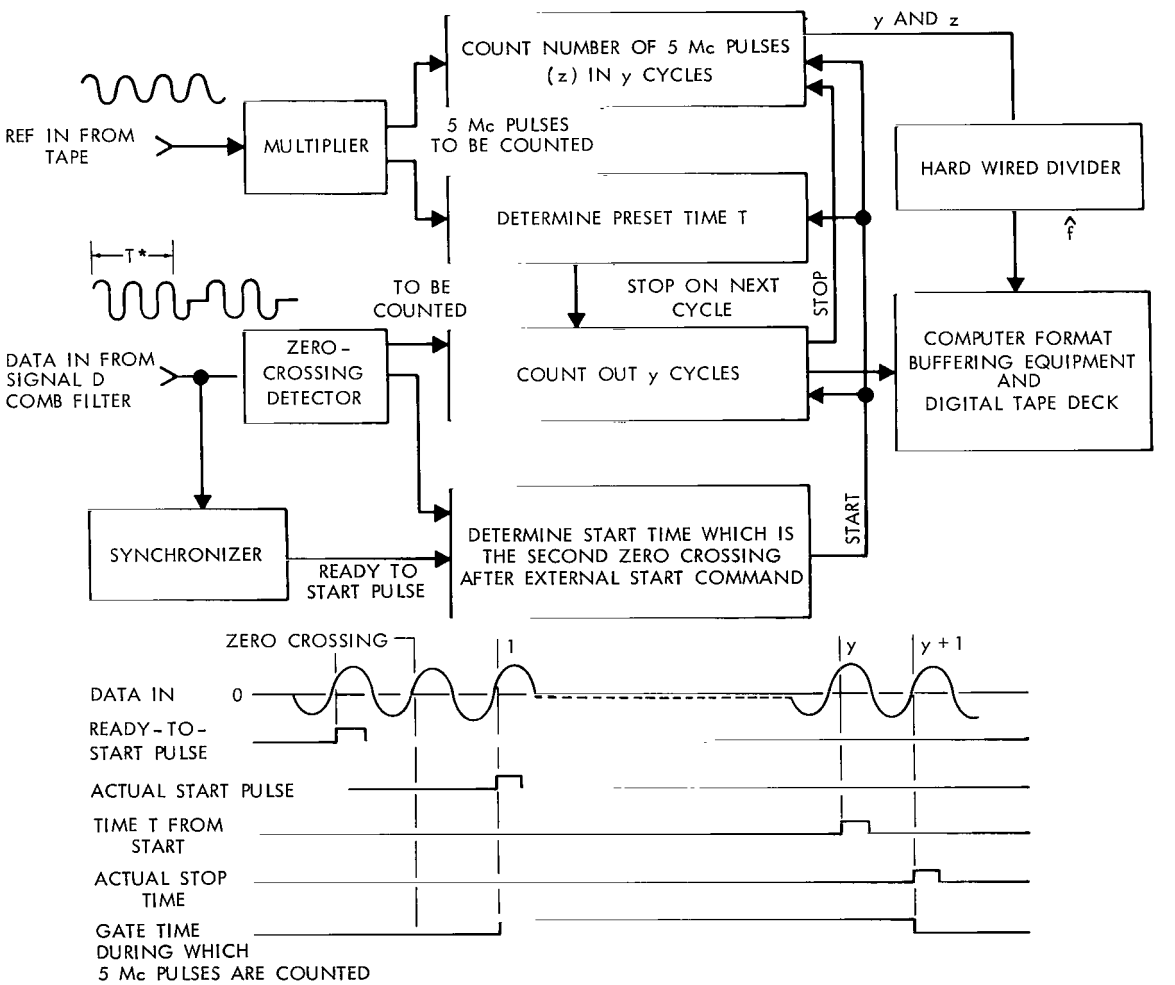

* T = 6.4ms for EDE-D
T = 1.0ms for ATS-B

Figure B1—HRP frequency measurement subsystem.

output of the device is 2 binary (or BCD) numbers, one indicating y, and the other indicating z (the number of 5-Mc pulses counted in exactly y cycles). The two numbers are then operated on by a hard wired divider to yield the frequency $\hat{f} = (y/z)\ (5 \times 10^6)$ cps.

The HRP is designed to process the analog data from a magnetic tape. To compensate for tape speed variation the processor clock frequency, which provides the count z, is generated by a frequency multiplier whose input is a reference frequency from the magnetic tape.

Appendix C

The Signal D Comb Filter

The block diagram of the Signal D comb filter is shown in Figure C1. The auction circuit allows only one output at one time to go to the FA flip flops. The FA's are sequentially strobed to discover whether one has an input. When the sequential strobe reaches an FA with an input indicated by its corresponding auction circuit, that FA is set, the strobes are stopped, and only the output from the filter corresponding to that FA is gated into the HRP input. Once the decision as to which filter should be gated out is made, it is irrevocable for that burst. Figure C2 is a timing diagram of the HRP Signal D comb filter for EPE-D nominal 5- to 15-kc, 55-cps channel rate.

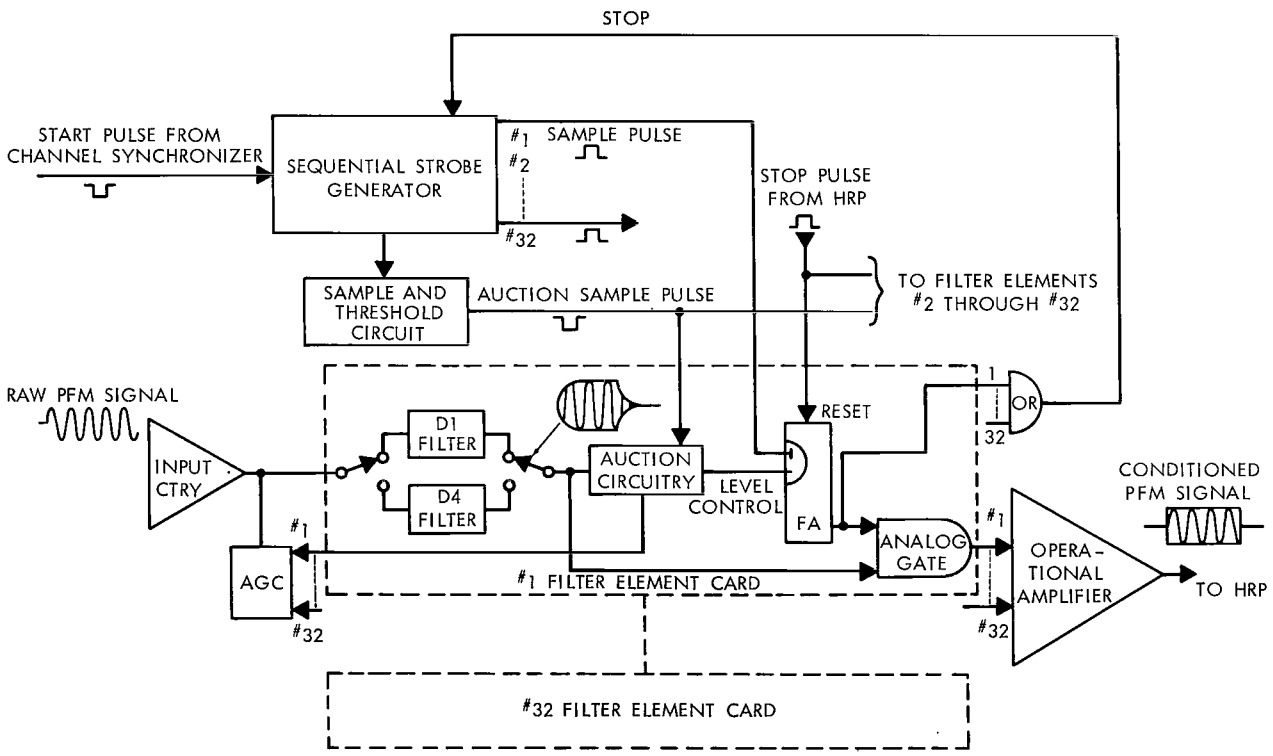

Figure C1—HRP Signal D comb filter block diagram.

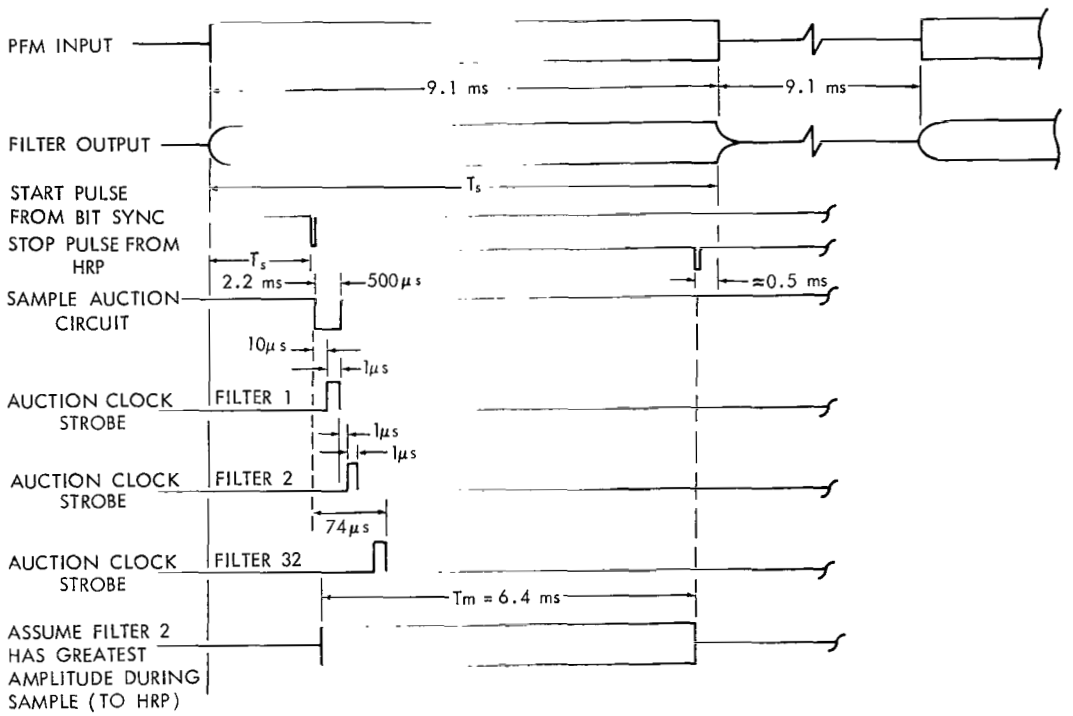

Figure C2—HRP Signal D comb filter timing diagram (nominal 5 kc to 15 kc data band, EPE-D).

Appendix D

Sample Calculation of Worst Case Expected Signal-to-Noise Ratio for AIMP-D

The real-time rate of AIMP-D is 1/16 of that used in the paper. The data band of 5 to 15 kc and an ENBW of 20 kc was used. In actual processing, these are the frequencies experienced because processing is performed at 16 times the real-time rate* for these satellite data.

An ENBW of 1250 cps (20 kc/16) is used in the following calculation to be consistent with the demodulated signal during transmission. It is less than the true noise bandwidth seen at the demodulator output, as should be the case.

The received signal P_s will be considered first:

$$P_s = P_T + G_T + G_R + L_P + L_x$$
$$= 36 \text{ dbm} - 7 \text{ db} + 22 \text{ db} - 188 \text{ db} - 6 \text{ db}$$
$$= -143 \text{ dbm}$$

where

P_s = received signal power

P_T = effective transmitting power (sideband power)

G_T = worse case transmitting antenna gain including passive element losses from the spacecraft to antenna

L_P = path loss, or free space attenuation when spacecraft is at apogee as given by $20 \log_{10} \lambda^2/(4\pi r)^2$ where λ is the carrier wavelength in meters and r is the slant range in meters

L_x = worse case operational contingency, or system operating margin.

The received noise power within 1250 cps ENBW is then calculated:

$$P_n = 10 \log_{10} k\,TB$$
$$= 10 \log (1.38 \times 10^{-23}) (945) (1250)$$
$$= -137.8 \text{ dbm},$$

*The demodulated carrier signal, the PFM signal, is recorded on analog tape at the telemetry receiving station. The same analog tape signal is reproduced at the Goddard Space Flight Center at 16 times the record rate for processing.

where

k = Boltzmann's constant

T = sum of disturbing noise temperatures in °K as follows:

Galactic noise* = 600°K
Earth and atmospheric noise = 55°K
Receiver noise = 290°K

B = ENBW, the equivalent noise bandwidth in cps.

The signal-to-noise ratio is

$$S/N]_{db} = P_s]_{dbm} - P_n]_{dbm}$$
$$= -143 - (-137.8)$$
$$= -5.2 \text{ db.}$$

At this low signal-to-noise ratio and ENBW, the noise introduced between the recording and reproducing process is negligible. Inspection of the performance curve for -5.2 db as given in Figure 11 then shows that a recovery of 99.8 percent can be expected given that the signal within the noise remains uniform.

The expected received signal-to-noise ratio of +6.5 db for the EPE-D spacecraft when at apogee was tabulated for a noise power equal to that used for AIMP-D for an ENBW of 20 kc and for:

P_T = 31 dbm

G_T = -4 db

G_R = 19 db

L_p = -164 db

L_x = -3 db.

The expected received signal-to-noise ratio of -3 db for the ATS-B spacecraft was tabulated for a noise power equal to that used for AIMP-D for an ENBW of 20 kc and for:

P_T = 33 dbm

G_T = -6 db

G_R = +22 db

*The galactic noise temperature is chosen as an expected average temperature. It does not include possible but improbable high noise situations such as could be received if the spacecraft background is the center of the galaxy or when the background is the region of the sun.

L_p = -169 db

L_x = -6 db.

These expected signal-to-noise levels are shown in Figure 11.

The performance transfer characteristics and the orbit-to-data recovery transfer characteristic curves for AIMP-D are shown in Figures D1 and D2, respectively. As can be seen, the signal-to-noise ratio changes 19 db from perigee to apogee. Also, AIMP-D spends most of the time at the poor signal-to-noise ratio. Figure D2 is the projection of the worst case theoretical received signal-to-noise ratio as applied to the F-8 actual performance curve. As can be seen, a 3-db change in the input signal-to-noise ratio causes data recovery to drop approximately 5 percent for this hypothetical example.

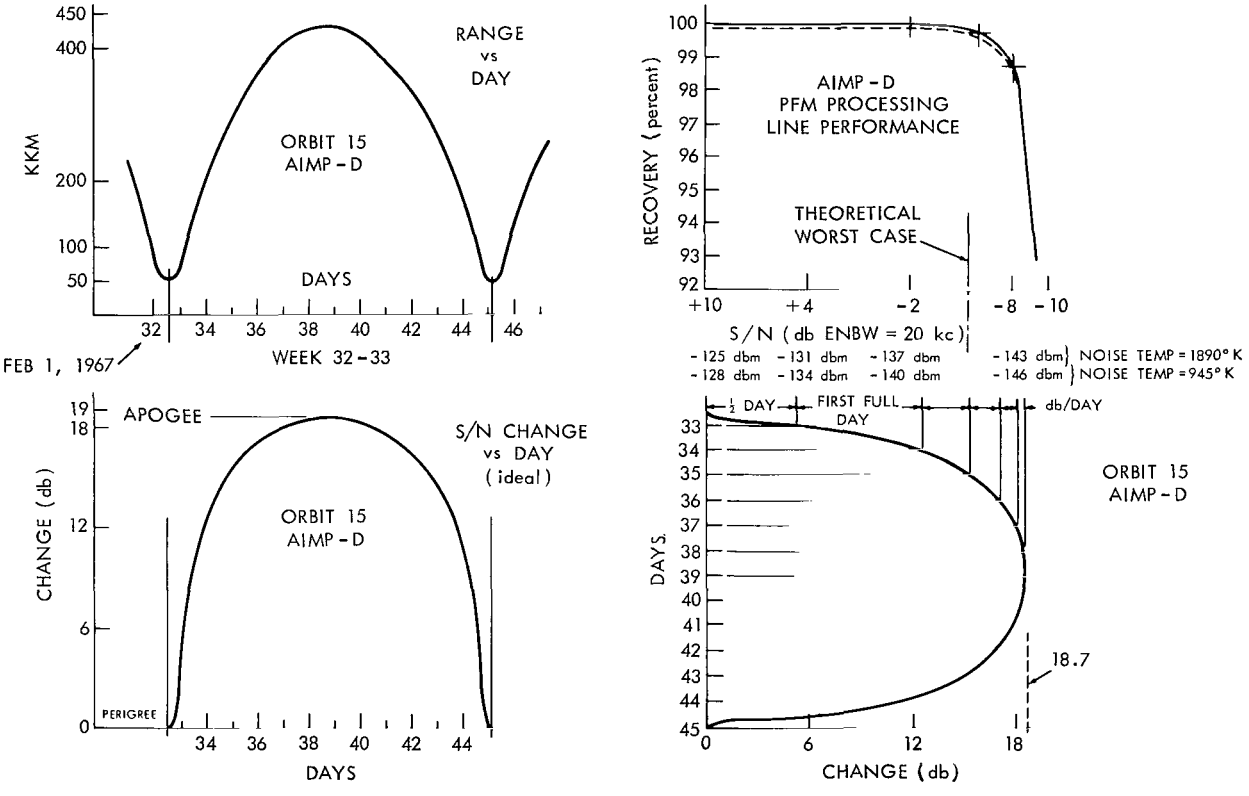

Figure D1—AIMP-D performance transfer characteristics.

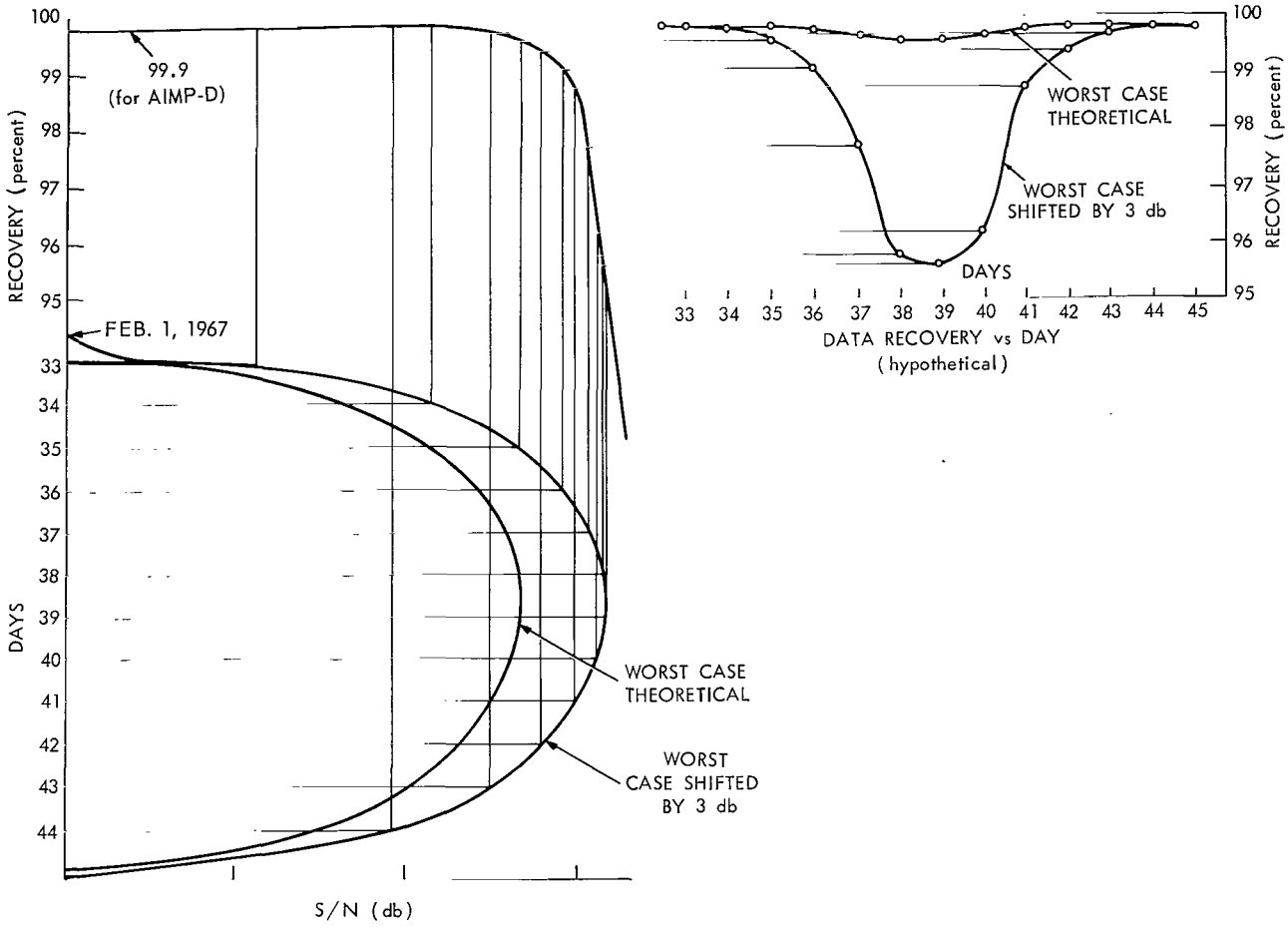

Figure D2—AIMP-D orbit-to-data recovery transfer characteristics.

05U 001 32 51 3DS 68059 00903
AIR FORCE WEAPONS LABORATORY/AFWL/
KIRTLAND AIR FORCE BASE, NEW MEXICO 87117

ATT MISS MADELINE F. CANOVA, CHIEF TECHNI
LIBRARY /WLIL/

"The aeronautical and space activities of the United States shall be conducted so as to contribute . . . to the expansion of human knowledge of phenomena in the atmosphere and space. The Administration shall provide for the widest practicable and appropriate dissemination of information concerning its activities and the results thereof."

—NATIONAL AERONAUTICS AND SPACE ACT OF 1958

NASA SCIENTIFIC AND TECHNICAL PUBLICATIONS

TECHNICAL REPORTS: Scientific and technical information considered important, complete, and a lasting contribution to existing knowledge.

TECHNICAL NOTES: Information less broad in scope but nevertheless of importance as a contribution to existing knowledge.

TECHNICAL MEMORANDUMS: Information receiving limited distribution because of preliminary data, security classification, or other reasons.

CONTRACTOR REPORTS: Scientific and technical information generated under a NASA contract or grant and considered an important contribution to existing knowledge.

TECHNICAL TRANSLATIONS: Information published in a foreign language considered to merit NASA distribution in English.

SPECIAL PUBLICATIONS: Information derived from or of value to NASA activities. Publications include conference proceedings, monographs, data compilations, handbooks, sourcebooks, and special bibliographies.

TECHNOLOGY UTILIZATION PUBLICATIONS: Information on technology used by NASA that may be of particular interest in commercial and other non-aerospace applications. Publications include Tech Briefs, Technology Utilization Reports and Notes, and Technology Surveys.

Details on the availability of these publications may be obtained from:

SCIENTIFIC AND TECHNICAL INFORMATION DIVISION

NATIONAL AERONAUTICS AND SPACE ADMINISTRATION

Washington, D.C. 20546